A&A 449, 41–48 (2006)
DOI: 10.1051/0004-6361:20053680

Astronomy & Astrophysics

Spectral indications of thermal Sunyaev-Zel'dovich effect in ARCHEOPS and WMAP data

C. Hernández-Monteagudo[1,2], J. F. Macías-Pérez[3], M. Tristram[3], and F.-X. Désert[4]

[1] Department of Physics & Astronomy, University of Pennsylvania, 209 South 33rd Str., Philadelphia, PA 19106, USA
[2] Max-Planck-Institut für Astrophysik, Karl-Schwarzschild-Str.1, Postfach 1317, 85741 Garching, Germany
e-mail: macias@lps.in2p3.fr
[3] Laboratoire de Physique Subatomique et Cosmologie, 53 Av. des Martyrs, 38026 Grenoble Cedex, France
[4] Laboratoire d'Astrophysique, Obs. de Grenoble, BP 53, 38041 Grenoble Cedex 9, France

Received 22 June 2005 / Accepted 21 November 2005

ABSTRACT

In this paper, we present a joint cross-correlation analysis of the ARCHEOPS CMB maps at 143 and 217 GHz and the WMAP CMB maps at 41, 61 and 94 GHz with sky templates of projected galaxy density constructed from the 2MASS Extended Source catalog. These templates have been divided in patches sorted in decreasing galaxy density with a fixed number of pixels (we considered patches having 32, 64 and 128 pixels) and the cross correlation has been performed independently for each of these patches. We find that the densest patch shows a strong temperature decrement in the Q, V, W bands of WMAP and in the 143 GHz channel of ARCHEOPS, but *not* in the 217 GHz channel. Furthermore, we find that the spectral behavior of the amplitude of this decrement is compatible with that expected for the non-relativistic thermal Sunyaev-Zel'dovich effect, and is incompatible (at 4.5σ level) with the null hypothesis of having only CMB, noise and a dust component ($\propto\nu^2$) in those pixels. We find that the first 32-pixel sized patch samples the cores of 11 known massive nearby galaxy clusters. Under the assumption that the decrement found in this patch is due entirely to the thermal Sunyaev-Zel'dovich effect, we obtain an average comptonization parameter for those sources of $y = (0.39 \pm 0.07) \times 10^{-4}$ at 13 arcmin angular scales. This value is compatible at 1-σ with the expectation, $y = 0.49 \times 10^{-4}$, from a model of the cluster flux number counts based on the standard Λ-CDM cosmology (Xue & Wu 2001). The observed value of y is slightly diluted when computed for the first patch of 64 and 128 pixels, presumably due to the inclusion of less massive clusters, and the dilution factor inferred is also compatible with the quoted model.

Key words. cosmology: cosmic microwave background – Galaxy: globular clusters: general

1. Introduction

The thermal Sunyaev-Zel'dovich effect (hereafter tSZ, Sunyaev & Zel'dovich 1980) constitutes a unique tool to explore the presence of baryons in the Universe. It arises as a consequence of the distortion that the black body spectrum of the Cosmic Microwave Background (CMB) radiation experiences when it encounters a hot electron plasma. In this Compton scattering, electrons transfer energy to the CMB radiation, generating an *excess* of high energy photons and a deficit in the low energy tail of the distribution. This photon reallocation translates into a frequency dependent change of the brightness temperature of the CMB, which, in the non-relativistic limit, has a very simple form, ($f_{\rm tSZ}(x) = x/\tanh[x/2] - 4$, with $x = h\nu/k_{\rm B}T_{\rm CMB}$ the adimensional frequency in terms of the CMB temperature monopole $T_{\rm CMB}$). The amplitude of this distortion is proportional to the electron pressure integrated along the line of sight ($\delta T_{\rm tSZ}/T_{\rm CMB} = f_{\rm tSZ}(x) \int {\rm d}r\ \sigma_{\rm T} n_{\rm e}\ k_{\rm B}T_{\rm e}/(m_{\rm e}c^2)$, with $\sigma_{\rm T}$ the Thomson cross section and $n_{\rm e}$, $T_{\rm e}$ and $m_{\rm e}$ the electron number density, temperature and mass, respectively); and this makes this effect particularly sensitive to collapsed or collapsing structures containing hot electrons, such as clusters and superclusters of galaxies (see Birkinshaw 1999, for a extensive review).

In addition to the intrinsic energy inhomogeneities of CMB radiation generated during inflation, there are further temperature anisotropies introduced in the CMB during recombination, which are mainly caused by two physical processes. These processes are the *last* Doppler kick exerted by electrons via Thomson scattering just before recombining, and the subsequent gravitational redshift experienced by CMB photons as they climb the potential wells generated by the inhomogeneities in the matter distribution (Sachs & Wolfe effect, e.g. Hu & Sugiyama 1995). While all this happens at $z \sim 1100$, a similar scenario can take place at much lower redshifts: as the first stars reionise the universe, new free electrons are produced which again scatter CMB photons, partially blurring primordial anisotropies generated during recombination and introducing new ones at much larger angular scales. Also, if Ω_Λ is non-zero, the decay of gravitational potentials in linear scales introduces a net blueshift in the CMB radiation at late epochs ($z < 2$), which is known as the Integrated Sachs Wolfe effect,

(ISW Sachs & Wolfe 1967). Despite the fact that most of these phenomena introduce temperature fluctuations of amplitudes larger than the tSZ effect, the particular frequency dependence of the latter should enable its separation. Whereas the first generation of CMB experiments like COBE (Smoot et al. 1991) and Tenerife (Gutiérrez et al. 2000) aimed to simply detect the largest CMB temperature anisotropies in the big angular scales, experiments like, e.g., Boomerang (Mauskopf et al. 2000), VSA (Rubiño-Martín et al. 2003), ARCHEOPS (Benoît et al. 2002) and WMAP (Bennett et al. 2003) have already reached the sensitivity and angular resolution levels required to probe relatively weak signals like the tSZ effect.

In this work we perform a combined analysis of ARCHEOPS and WMAP CMB data, searching for *spectral* signatures of the tSZ effect. Previous works (Bennett et al. 2003; Hernández-Monteagudo & Rubiño-Martín 2004; Myers et al. 2004; Hernández-Monteagudo et al. 2004; Afshordi et al. 2004; Fosalba et al. 2003; Fosalba & Gaztanaga 2004) have claimed the detection of tSZ in WMAP data at different significance levels. However, all those studies were exclusively based on spatial cross-correlations of large scale structure catalogues with CMB data. In this work, we take advantage of the frequency coverage provided by the combination of ARCHEOPS and WMAP experiments in order to include an analysis of the frequency behavior of a signal which is spatially correlated with regions hosting large galaxy overdensities.

The sketch of the paper is as follows: in Sect. 2 we summarize the outcome of the ARCHEOPS and WMAP experiments, whose data products are analyzed as explained in Sect. 3. Section 4 shows our results, which are compared with those obtained from WMAP data. Their implications are discussed in Sect. 5. Finally, we conclude in Sect. 6.

2. The ARCHEOPS and WMAP data set

The ARCHEOPS (Benoît et al. 2002)[1] experiment was designed to obtain a large sky coverage of CMB temperature anisotropies in a single balloon flight at millimeter and submillimeter wavelengths. ARCHEOPS is a precursor to the PLANCK HFI instrument (Lamarre et al. 2003), using the same optical design and the same technology for the detectors, spider–web bolometers, and their cooling 0.1 K dilution fridge. The instrument consists of a 1.5 m aperture diameter telescope and an array of 21 photometric pixels operating at 4 frequency bands centered at 143, 217, 353 and 545 GHz. The two low frequencies are dedicated to CMB studies while high frequency bands are sensitive to foregrounds, essentially to interstellar dust and atmospheric emission. Observations are carried out by spinning the payload around its vertical axis at 2 rpm. Thus the telescope produces circular scans at a fixed elevation of ∼41 deg. The data were taken during the Arctic night of February 7, 2002 after the instrument was launched by CNES from the Esrange base near Kiruna (Sweden). The entire data set covers ∼30% of the sky in 12 h of night observations.

For the purpose of this paper, we concentrate in the low frequency channels at 143 and 217 GHz. Maps for each of the bolometers have been produced from the ARCHEOPS processed and foreground cleaned timelines, using the Mirage optimal map making code (Yvon & Mayet 2005) as discussed in (Tristram et al. 2005). The maps for the 4 most sensitive bolometers at 143 GHz were combined into a single map at 143 GHz and equally the two most sensitive bolometer maps were combined at 217 GHz. The CMB dipole is the prime calibrator of the instrument. The absolute calibration error against the dipole as measured by COBE/DMR (Fixsen et al. 1994) and confirmed by WMAP (Bennett et al. 2003) is estimated to be 4% and 8% in temperature at 143 GHz and 217 GHz respectively. These errors are dominated by systematic effects. The noise contribution in the combined maps at 143 and 217 GHz was computed using Monte Carlo simulations. For each bolometer, by using the power spectrum of the noise in the time domain data set, we produced fake timelines of ARCHEOPS noise. These were processed and projected into maps following the same procedures used for the ARCHEOPS data themselves as described before.

The WMAP satellite mission was designed to measure the CMB temperature and polarization anisotropies in 5 frequency bands, 23, 33, 41, 61 and 94 GHz with a full sky coverage. The satellite was launched in June 2001 and its first results after the first year of observations (Bennett et al. 2003) included the CMB temperature and temperature-polarization cross-correlation power spectra, as well as full sky temperature maps for each of the frequency bands. In this paper we consider only data from the high frequency channels, Q [41 GHz], V [61 GHz] and W [94 GHz], since only for these bands there are foreground clean maps available at the LAMBDA site `http://lambda.gsfc.nasa.gov/`

3. The statistical analysis

In this section we outline the correlation analysis performed on ARCHEOPS and WMAP data and the 2MASS Extended Source Catalog (XSC, Jarrett et al. 2003) on the sky region covered by ARCHEOPS. This analysis is essentially identical to that applied in (Hernández-Monteagudo et al. 2004), paper to which we refer for a more detailed description of the statistical method. It consists of a pixel-to-pixel comparison of the CMB data with a template of the large scale structure built from the 2MASS XSC catalog.

The 2MASS XSC catalog contains approximately 1.6 million galaxies detected in the infrared filters I, J and K, and covers the whole celestial sphere. Those frequencies are particularly insensitive to dust absorption, and for this reason this catalog can trace the extragalactic structure at very low galactic latitudes. The galaxy templates built from it take into account the spatial distribution of the galaxies and the instrumental beam of the CMB experiment. By using the HEALPix[2] (Górski et al. 1999) tessellation of the sky, we built a map with the same resolution parameter ($N_{\rm side} = 512$) than the one used in ARCHEOPS and WMAP data. Every pixel was assigned a value equal to the number of galaxies present in such pixel.

[1] See `http://www.archeops.org`

[2] HEALPix's URL site:
`http://www.eso.org/science/healpix/`

The resulting map was then convolved with a window function corresponding to the instrumental beam of each of the detectors taken into consideration. For ARCHEOPS, the resulting templates were then weighted by their noise levels and co-added per frequency band, in such a way that we ended up with two different galaxy templates corresponding to the 143 GHz and 217 GHz bands. For WMAP, we produced templates for the Q, V and W bands.

In the next step, we sorted the pixels of each template in terms of its amplitude, so that *first* pixels would have *higher* galaxy densities. These pixels were grouped in patches of varying sizes (32, 64 or 128 pixels per patch), and again patches were sorted in such a way that first patches contained larger projected galaxy densities. Next, we analyzed *each* of these patches separately, by comparing them to the corresponding patches in the ARCHEOPS and WMAP CMB maps on a pixel-to-pixel basis.

As explained in e.g. (Hernández-Monteagudo & Rubiño-Martín 2004), it is possible to estimate the contribution of a given spatial template ($\mathbf{M}$) on a total measured temperature map ($\mathbf{T}$), which is the result of the addition of several components:

$$\mathbf{T} = \mathbf{T}_{\rm cmb} + \tilde{\alpha} \cdot \mathbf{M} + \mathbf{N}, \quad (1)$$

namely CMB ($\mathbf{T}_{\rm cmb}$), instrumental noise ($\mathbf{N}$) and some signal coming from the extragalactic template ($\mathbf{M}$). The contribution of $\mathbf{M}$ is parametrized by $\tilde{\alpha}$, and an optimal value of it (*optimal* in terms of the temperature model given in Eq. (1)), together with its formal error bar, is given by

$$\alpha = \frac{\mathbf{T}C^{-1}\mathbf{M}^T}{\mathbf{M}C^{-1}\mathbf{M}^T}, \quad \sigma_\alpha = \sqrt{\frac{1}{\mathbf{M}C^{-1}\mathbf{M}^T}}. \quad (2)$$

The matrix C is the covariance matrix of $\mathbf{T}$, which must contain the correlation matrices of both the CMB and noise components. For the small scales we are probing here (the pixel has a size of ∼7 arcmin), the noise is the main contributor to the covariance matrix[3]. In our case, this matrix must be evaluated *only for the pixels belonging to the patch under analysis*. Since our patches are relatively small, the inversion of this matrix poses no numerical problem.

Therefore, for every patch a value of α and σ_α was obtained. However, uncertainties in the determination of the noise amplitude may bias our determination of σ_α, and for this reason we computed a different estimate of the uncertainty of α, namely the rms variation of this parameter for all available patches, which will be denoted as $\sigma_\alpha^{\rm rms}$. We remark the fact that, according to Eq. (2), an error in the noise normalization does not affect the estimates of α, but only those of σ_α. When comparing σ_α with $\sigma_\alpha^{\rm rms}$, we found that for the 143 GHz channel of ARCHEOPS, the latter was about a 40% larger than the former, and hence we decided to adopt it in order to quote conservative estimates of statistical significance. For the 217 GHz case no such bias was found, and we decided to use again $\sigma_\alpha^{\rm rms}$.

[3] Note that for these small scales, the assumption of a Poissonian noise is a good approximation.

4. Combined results for ARCHEOPS and WMAP

In Fig. 1 we plot the recovered α's versus the patch index. Results are grouped in six different panels: top and bottom panels refer to WMAP and ARCHEOPS experiments, respectively, whereas left, middle and right panels display results for patches of 32, 64 and 128 pixels, respectively. For ARCHEOPS, filled circles and diamonds refer to 143 GHz and 217 GHz respectively, whereas for WMAP those symbols correspond to the W and the Q channels, being the results of the V band given by the crosses. Dark and light grey colored bands limit the 2-σ confidence levels for filled circles and diamonds, respectively, while the moderately dark bands refer to the V band (crosses) in the case of WMAP. As explained above, for the 143 GHz and 217 GHz channels the amplitude of the shaded regions was computed from the typical dispersion of the values obtained for α in patches where the tSZ contribution is expected to be negligible, i.e., in patches with indexes between 40 and 300. We have found that for the 143 GHz channel the first patch contains an unusual negative α while at 217 GHz seems to be compatible with zero. This patch, in the case it contains 64 pixels, hosts the central pixels of 20 different ACO clusters of galaxies, COMA among them. Out of them, 11 (COMA again included) are already sampled by the 32 densest pixels. Its statistical significance is slightly bigger for patches with 64 pixels (>2.5-$\sigma^{\rm rms}$), since it contains the first two *very negative* patches of 32 pixels each, (see Fig. 1d). In Fig. 1e, from the first 300 patches, very few of them (∼12) depart from zero by an amount similar to that of the first patch; and such number is very close to what one expects under Gaussian statistics at 2.5-σ level of significance. This peculiar behavior of the first (or first two) patch(es) disappears at 217 GHz (see diamonds): in no case the diamonds corresponding to the first two patches trespass the 2-$\sigma^{\rm rms}$ limit. This picture is consistent with part of the signal being generated by the tSZ effect, since such component is negative at 143 GHz and becomes zero at 217 GHz.

In order to interpret the results from WMAP, one musts keep in mind that the Q and V bands have remarkably larger beams than the W band: while the ARCHEOPS' and W band's Point Spread Functions are similar in size (≈13 arcmin), the beams of the Q and V bands have an average (linear) size of ∼31 and 21 arcmin respectively. This, in terms of tSZ flux, corresponds to factors ∼5.7 and 2.6 smaller in the Q and V band for point-like objects. On the other hand, it is clear from Fig. 1 that WMAP has a much lower noise level when compared to ARCHEOPS, (approx. a factor of 3.5). As one looks at the top panels in Fig. 1, one finds that for the first patch of both 32 and 64 pixel size, the W band gives a decrement about 4-σ away from zero, (which however is not found for the second patch of 32 pixel size). This statistical singularity of the first patch decreases remarkably in the Q and V bands, but still remains close to the 2-σ level. However, due to the argument on beam dilution on bands Q and V with respect to W, we still find the amplitudes given by the three bands of WMAP consistent with being (at least partially) generated by unresolved objects causing a temperature decrement.

It also worth to remark that, if the first patch contains pixels which do *not* contribute considerably to the tSZ decrement,

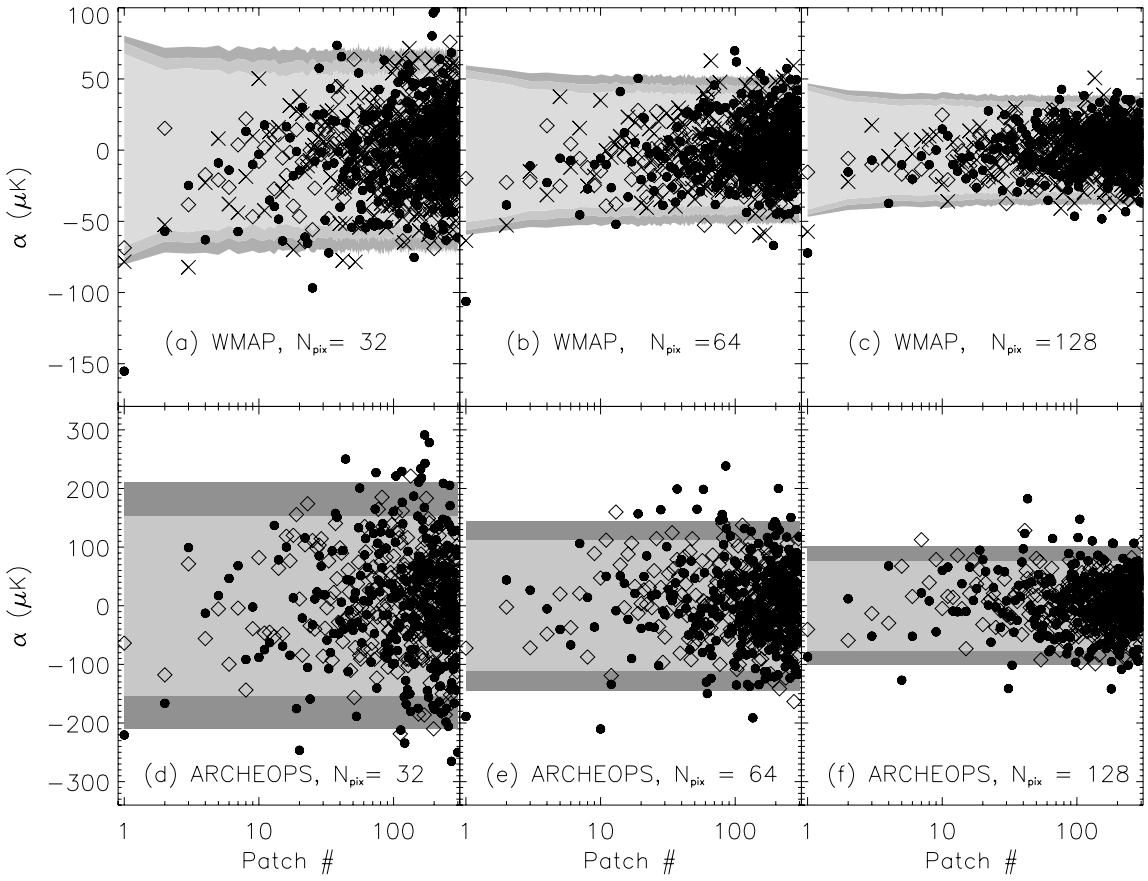

Fig. 1. α's obtained by means of Eq. (2) from ARCHEOPS and WMAP data in the fraction of the sky covered by the former experiment. In panels **a)–c)**, filled circles, crosses and diamonds refer to the W, V and Q bands respectively. In panels **d)–f)**, the 143 GHz and 217 GHz channel results are given by filled circles and diamonds, respectively. The colored bands display the 2-σ confidence limit for the α's: dark grey for filled circles, intermediate grey for crosses, and light grey for diamonds. Our analysis are focused on the first patch, hosting the highest projected galaxy density.

the significance of the overall α obtained for that patch will diminish accordingly. This is our explanation for the decreasing significance of the values of α in the first patch for a size of 128 pixels when compared to a size of 64 pixels.

5. Discussion

5.1. Spectral dependence of the cross-correlation coefficients

As discussed in the previous section, Fig. 1 indicates a significant temperature decrement in patch 1 for both the ARCHEOPS and WMAP data sets which seems to be compatible with the tSZ effect. For a better assessment of this result we have compared, via a linear fit, the observed spectral dependency of the correlation coefficients α in each of the patches to the following model

$$\alpha(\nu) = A \times f_{\rm tSZ}(\nu) + n(\nu) \quad (3)$$

where A is global calibration factor which is estimated from the fit, $f_{\rm tSZ}(\nu)$ represents the spectral behavior of the tSZ-induced change in brightness temperature and $n(\nu)$ is the instrumental noise in $\alpha(\nu)$. For this model if the signal observed is compatible with the tSZ effect we expect a temperature decrement and A to be significantly positive, otherwise we expect no correlation and therefore A to be compatible with zero. We must remark that, due to the different size of the beams for every channel, we had to rescale the α's to a common reference beam size of 13 arcmin. When doing this, we assumed that the signal was generated by unresolved sources, and hence we scaled the α's as the ratio of the area of the beam with the reference one.

The main results of the fitting procedure described before are shown in Fig. 2 where we trace the fitted amplitude, A, of the tSZ signal as a function of the patch number for patches of 32 pixels. We observe that only for patch number 1, where most massive clusters might be, there is a significant temperature decrement ($A > 0$). For a closer look to the fits, Figs. 3–5 represent the α coefficient in CMB temperature units as function of frequency in GHz for the 32, 64 and 128 pixel patches respectively. The top plot corresponds to patch 1 and the bottom one to a patch containing an average value of the projected galaxy density (patch 201). In the three figures we observe that the correlation coefficients found for the patch 1 are consistent which what we expect for tSZ emission with A values of

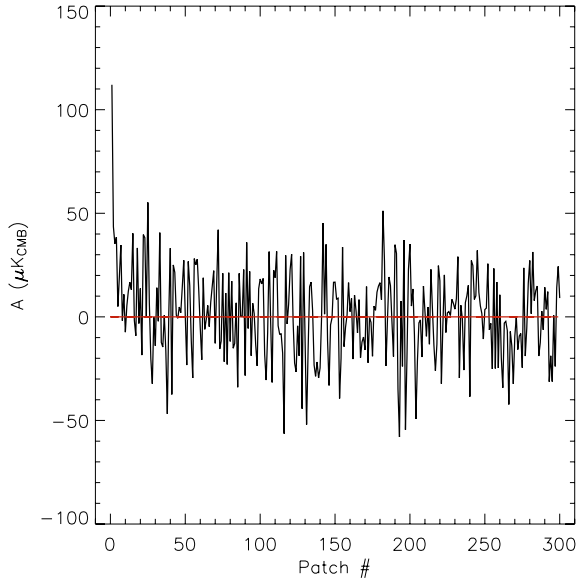

Fig. 2. tSZ fitted amplitude, A, as a function of patch number. We only observe a significant temperature decrement ($A > 0$) in patch number 1.

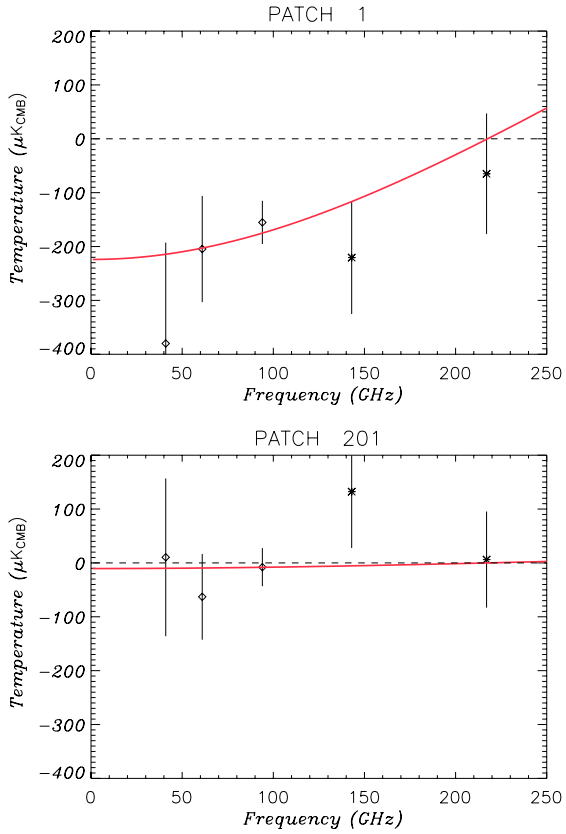

Fig. 3. The α correlation coefficient in CMB temperature units as function of frequency in GHz for patch 1 (*top panel*) and patch 201 (*bottom panel*) of the 32 pixel patches. The diamonds are the WMAP data points and the stars the ARCHEOPS one. In red, we overplot the best-fit tSZ computed as discussed in the text.

$106 \pm 21\ \mu$K, $73 \pm 15\ \mu$K and $51 \pm 12\ \mu$K respectively. Notice as well that there is good agreement between the model and the data with reduced χ^2 values of 2/4, 2.6/4 and 2/4 for patches containing 32, 64 and 128 pixels respectively. For the null hypothesis ($A = 0\ \mu$K), the reduced χ^2 values are 28/5, 26/5 and 20/5. We interpret these results as a spectral indication of the measurement of a tSZ signal in patch 1. However, for all other patches we find A compatible with zero, showing that the data are in good agreement with the null hypothesis. For example, for patch 201 the A values are $-19 \pm 19\ \mu$K, $-4 \pm 13\ \mu$K and $10 \pm 9\ \mu$K with reduced χ^2 values of 2.2/4, 1.2/4 and 1.3/4 respectively. We consider these results compatible with a no detection of tSZ signal in patch 201.

The uncertainties for the total amplitude of the tSZ signal, A, presented above do not account for systematic errors on the ARCHEOPS data. These are dominated by residuals from atmospheric and Galactic dust emissions which in a first order approximation increase as ν^2 in the ARCHEOPS frequency range. To account for those contributions we have recomputed the total amplitude for the tSZ signal adding an extra term in the fitted function as follows:

$$\alpha(\nu) = A \times f_{\rm tSZ}(\nu) + A_{\rm sys} \times \nu^2 + n(\nu), \quad (4)$$

where $A_{\rm sys}$ is computed only from the ARCHEOPS data. For patch 1 we obtain A values of $110 \pm 22\ \mu$K, $74 \pm 16\ \mu$K and $53 \pm 12\ \mu$K, and $A_{\rm sys}$ values of $-95 \pm 102\ \mu$K, $-104 \pm 71\ \mu$K and $-46 \pm 51\ \mu$K for patches of 32, 64 and 128 pixels respectively. From these results we conclude that the A coefficients are not significantly affected at 1-σ level by systematic effects present in the ARCHEOPS data.

We have repeated the previous analyses using WMAP data only. The results obtained are fully compatible within the error bars with those obtained using Archeops and WMAP data combined. The error bars for the WMAP only case are about 10% larger. One must keep present that the WMAP data point at 94 GHz has a significantly smaller error bar than all other points and that hence it dominates the fit.

5.2. Determination of the mean and integrated Compton parameters

It is interesting to check whether pixels in patch 1 correspond to potential sources of tSZ or not. For the 32-pixel-size patches, patch 1 includes COMA, A0576, A0671, A0952, A1795, A2061, A2065, A2244, A2245, A2249, A2255. Since these are massive and relatively nearby galaxy clusters, it is reasonable to expect some signature of the tSZ effect. It might occur, however, that our evidence for tSZ signal is mainly caused by COMA, which is a nearby very massive cluster whose tSZ signature has been studied extensively (Battistelli et al. 2003). We have repeated our analyses after masking out all pixels lying within a radius of 2.5° from COMA cluster's center and found that our tSZ amplitudes decreased typically by a 10%–15%, but still being statistically significant. This demonstrates that the presence of COMA is not critical to our results. Using the quoted values for the A parameter we infer the following estimate for the average Compton parameter in the source quoted above: $y = (0.39 \pm 0.07) \times 10^{-4}$. In the case of 64-pixel-size patches we have roughly the same clusters and we expect

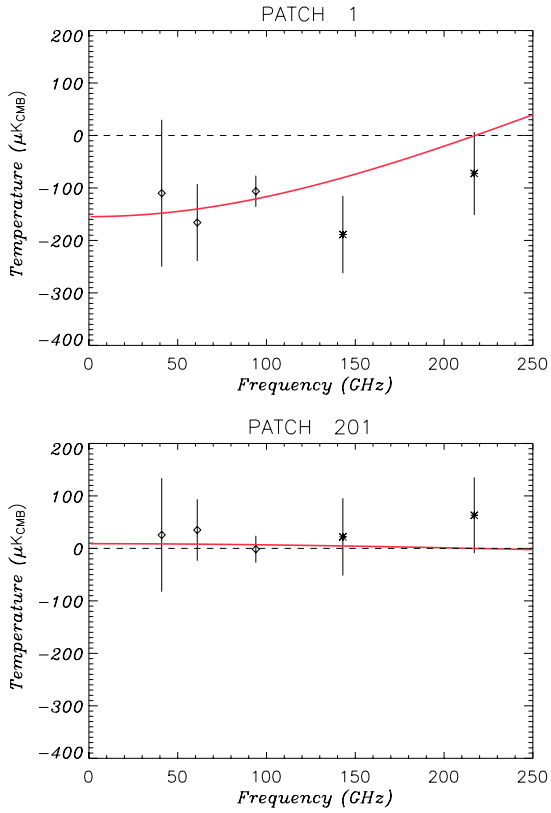

Fig. 4. α correlation coefficient in CMB temperature units as function of frequency in GHz for patch 1 (*top panel*) and patch 201 (*bottom panel*) of the 64 pixel patches. The diamonds are the WMAP data points and the stars the ARCHEOPS one. In red, we overplot the best-fit tSZ computed as discussed in the text.

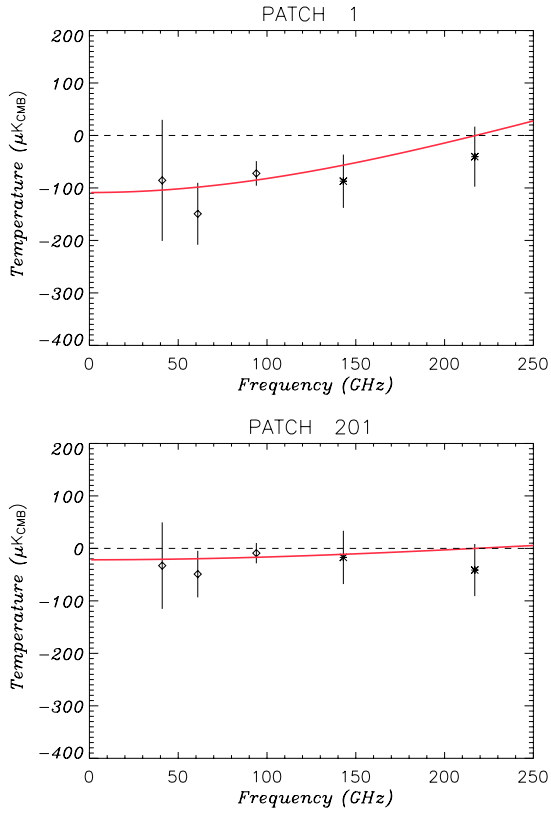

Fig. 5. The α correlation coefficient in CMB temperature units as function of frequency in GHz for patch 1 (*top panel*) and patch 201 (*bottom panel*) of the 128 pixel patches. The diamonds are the WMAP data points and the stars the ARCHEOPS one. In red, we over plot the best-fit tSZ computed as discussed in the text.

therefore the signal to be diluted, $y = (0.27 \pm 0.06) \times 10^{-4}$. Finally for 128 pixel-size patches, patch 1 includes the following 27 clusters: COMA, A0077, A0104, A0272, A0376, A0407, A0576, A0671, A0952, A1035, A1185, A1235, A1377, A1767, A1795, A1800, A2034, A2061, A2065, A2069, A2142, A2151, A2199, A2244, A2245, A2249, A2255. We deduce for them $y = (0.19 \pm 0.04) \times 10^{-4}$. Since we have scaled the α's to the beam-size of the 143 GHz channel of ARCHEOPS, these quoted values of y are associated to a (linear) angular scale on the sky of ∼13 arcmin. For the above results we have assumed the CMB temperature to be $T_{\rm CMB} = 2.725$ K (Mather et al. 1999).

We now try to relate the observed average tSZ decrement $\langle y_{\rm obs} \rangle$ to the high end of the SZ number counts. We make 2 hypotheses: 1) that the Archeops beam encloses most of the integrated tSZ effect in clusters and 2) that the 2MASS survey is a perfect tracer of the tSZ effect. We will come back to these hypotheses at the end.

The correlation analysis, that is presented in the previous section, can be recast in stating that the $N_{\rm pix}$ brightest clusters of galaxies have an average integrated $Y = \int {\rm d}\Omega y$ parameter equal to $Y = \langle y_{\rm obs} \rangle \Omega_{\rm beam}$ where $\Omega_{\rm beam} = 2\pi(FWHM/\sqrt{8\log 2})^2$ is the Archeops beam solid angle if $FWHM = 13$ arcmin. The integrated Compton parameter can be directly related to the SZ flux number counts which has been the issue of a great number of studies (e.g. Aghanim et al. 1997; Bartlett et al. 1994; Barbosa et al. 1996; Bartelmann et al. 2001) from which we select (Xue & Wu 2001) and (Benson et al. 2002).

Following (Xue & Wu 2001) there are three possible models for which the number counts of clusters over the whole sphere can be parametrized in terms of Y as follows,

$$N(>Y) = N_0 (Y/Y_0)^{-\gamma}, \tag{5}$$

where we fiducially consider $Y_0 = 10^{-2}$ arcmin^2

For Model 1 (M1), deduced from the cosmological ΛCDM matter power spectrum, $N_0 = 29$ and $\gamma = 1.5$. For Model 2 (M2), a non-evolving X-ray luminosity function is used to correct the counts and gives a larger $N_0 = 635$ with the same exponent. Note that (Rubiño-Martín & Sunyaev 2003) also find this exponent when studying the number counts of high flux galaxy clusters). Finally Model 3 (M3), an evolving X-ray luminosity function is used instead, giving $N_0 = 350$ with a flatter exponent $\gamma = 1.2$. The conversion from flux in Jansky units to the Compton frequency-independent quantity Y is obtained via

$$\frac{F_\nu}{Y} = T_{\rm CMB} \frac{\partial B_\nu}{\partial T_{\rm CMB}} f_{\rm tSZ}(\nu). \tag{6}$$

For example, the fiducial value $Y_0 = 10^{-2}$ arcmin^2 is equivalent to 0.75 and 0.91 Jy at 90 and 143 GHz (resp.).

Table 1. Expected average Compton parameter, $\langle y \rangle / 10^{-4}$, in patch 1, as a function of the number of pixels in the patch for the four number counts models discussed in the text, M1, M2 and M3 Xue & Wu (2001) and B Benson et al. (2002).

Npix	CMB Data	M1	M2	M3	B
32	(0.39 ± 0.07)	0.49	3.91	6.24	2.02
64	(0.27 ± 0.06)	0.31	2.46	3.50	1.27
128	(0.19 ± 0.04)	0.19	1.55	1.96	0.80

From the above formulas, we deduce the lower limit $Y_{\rm min}$ in the number counts for the first $N_{\rm cl} = 32, 64, 128$ brightest clusters as

$$Y_{\rm min} = Y_0 \left(\frac{N_{\rm cl}}{N_0 f_{\rm sky}} \right)^{-1/\gamma} \tag{7}$$

where $f_{\rm sky} \sim 0.20$ is the effective sky fraction used in the Archeops–WMAP tSZ cross analysis. The average Y value of these clusters is then

$$\langle Y \rangle = Y_0 \frac{\gamma}{\gamma - 1} \left(\frac{N_{\rm cl}}{N_0 f_{\rm sky}} \right)^{-1/\gamma} . \tag{8}$$

We deduce the average Compton parameter for those clusters $\langle y \rangle$ as

$$\langle y \rangle = \frac{\langle Y \rangle}{2\pi (FWHM / \sqrt{8 \log 2})^2} . \tag{9}$$

For the previous three models, expected values for $\langle y \rangle$ are between 0.5×10^{-4} and 6×10^{-4}. The value expected from basic principles (M1), $\langle y \rangle = 0.49 \times 10^{-4}$, is quite close to the observed value $\langle y \rangle_{\rm obs} = 0.39 \pm 0.07 \times 10^{-4}$. The observed value should however be corrected up-wards. Non-linearities in the relation between the 2-MASS density field and the Y parameter introduce an efficiency which is difficult to estimate, although we note that as discussed above most of the brightest pixels in the density map constructed from the 2-MASS survey are associated to well-known clusters of galaxies. If we considered that only identified clusters (11) are present in the first patch of 32 pixels, the above expected values should be multiplied by a factor of two. Extension of the bright clusters beyond the fiducial beam of 13 arcmin (like Coma) may produce a differential effect with the observing beam at different frequencies, as well as a bias in the number counts.

We also note that the dependence of $\langle y \rangle$ with the number of pixels taken in the analysis (32, 64 or 128) follows quite well the Model 1 prediction as shown in Table 1. We have also cross-checked the (Xue & Wu 2001) modeling with that from (Benson et al. 2002). This alternative model produces an intermediate value between models M1 and M2 and is marginally compatible with the observations.

6. Conclusion

In this paper we have presented a joint cross-correlation analysis of the ARCHEOPS and WMAP data sets with a template of galaxy density constructed from the 2MASS XSC galaxy catalog. We have first divided the 2MASS sky density map in patches of equal number of pixels and sorted these patches in terms of decreasing projected galaxy density. For each of these patches we have performed a cross-correlation analysis with the ARCHEOPS data at 143 and 217 GHz and with the WMAP data for the Q, V and W bands. For patches containing the densest 32, 64 and 128 pixels (patch 1), the correlation test pointed to a prominent temperature decrement in WMAP's Q, V and W bands and in the 143 GHz band of ARCHEOPS, but *not* at 217 GHz, as would be expected for tSZ-induced temperature fluctuations. All the other patches failed to show a similar behavior.

To corroborate these results, for each of the patches we have compared the cross-correlation coefficients to a model of the tSZ frequency pattern, in which we fix the spectral behavior and fit for a global amplitude parameter A. For the first patch and the three sizes considered (32, 64 and 128 pixels), we obtain non zero A values at more than 4.5-σ level with good agreement between the model and the data, and negligible contribution from systematic residuals in the Archeops data. For all other pixels having smaller projected galaxy density, we fail to detect any signature of tSZ effect.

From these results, we conclude that there is clear indication of tSZ effect for patch 1 in the ARCHEOPS and WMAP data sets. This is not surprising, since patch 1 contains pixels centered in massive and relatively nearby galaxy clusters. Assuming the signal observed is tSZ, we infer, for the 32-pixels case, an average value for the comptonization parameter of $y = (0.39 \pm 0.07) \times 10^{-4}$ in all those clusters at an angular scale of $\sim$13 arcmin. This value is compatible at 1.5-σ level with the expectations, $y = 0.49 \times 10^{-4}$ (cf. Table 1), from a model of the cluster flux number counts based on the standard Λ-CDM model, M1, assuming the measured y is due to the contribution from the 32 brightest clusters. For 64 and 128-pixeles patches the tSZ signal is diluted, probably due to the contribution of relatively not so massive clusters. Note that the dilution observed is also compatible with the one expected from the model M1 (cf. Table 1).

Acknowledgements. We acknowledge the Archeops collaboration for the use of the proprietary Archeops data and for fruitful comments and careful reading of this manuscript. We acknowledge very useful comments by J.A. Rubiño-Martín. C.H.M. acknowledges the financial support from the European Community through the Human Potential Programme under contract HPRN-CT-2002-00124 (CMBNET). C.H.M. is currently supported by NASA grants ADP03-0000-0092 and ADP04-0000-0093. We acknowledge the use of the Legacy Archive for Microwave Background Data Analysis (LAMBDA, `http://lambda.gsfc.nasa.gov`). Support for LAMBDA is provided by the NASA Office of Space Science. This publication makes use of data products from the Two Micron All Sky Survey, which is a joint project of the University of Massachusetts and the Infrared Processing and Analysis Center/California Institute of Technology, funded by the National Aeronautics and Space Administration and the National Science Foundation. Some of the results in this paper have been derived using the HEALPix package, (Górski et al. 1999).

References

Afshordi, N., Lin, Y.-T., & Sanderson, A. J. R. 2005, ApJ, 629, 1A

Aghanim, N., De Luca, A., Bouchet, F. R., Gispert, R., & Puget, J. L. 1997, A&A, 325, 9

Amblard, A., & Hamilton, J. C. 2004, A&A, 417, 1189

Barbosa, D., Bartlett, J. G., Blanchard, A., & Oukbir, J. 1996, A&A, 314, 13

Barkats, D., Bischoff, C., Farese, P., et al. 2005, ApJ, 619, 127

Bartelmann, M. 2001, A&A, 370, 754

Bartlett, J. G., & Silk, J. 1994, ApJ, 423, 12

Battistelly, E. S., De Petris, M., Lamagna, L., et al. 2003, ApJ, 598, L75

Bennett, C. L., Hinshaw, G., Banday, A., et al. 1993, ApJ, 414, L77

Bennett, C. L., Halpern, M., Hinshaw, G., et al. 2003, ApJ, 148, 1

Benoît, A., Ade, P., Amblard, A., et al. 2002, APh, 17, 101

Benoît, A., Ade, P., Amblard, A., et al. 2003a, A&A, 399, L19

Benoît, A., Ade, P., Amblard, A., et al. 2003b, A&A, 399, L25

Benson, A. J., Reichardt, Ch., & Kamionkowski, M. 2002, MNRAS, 331, 71

de Bernardis, P., Ade, P. A. R., Bock, J. J., et al. 2000, Nature, 404, 955

Birkinshaw, M. 1999, PhR, 310, 97

Fixsen, D. J., Cheng, E. S., Cottingham, D. A., et al. 1994, ApJ, 420, 445

Fosalba, P., Gaztañaga, E., Castander, F. J., et al. 2003, ApJ, 597, L89

Fosalba, M. , & Gaztanaga, E. 2004, MNRAS, 350, L37

Górski K. M., Hivon E., & Wandelt, B. D. 1999, in Proceedings of the MPA/ESO Cosmology Conference, Evolution of Large-Scale Structure, ed. A. J. Banday, R. S. Sheth, & L. Da Costa, PrintPartners Ipskamp, NL, 37 (also [arXiv:astro-ph/9812350])

Gutiérrez, C. M., Rebolo, R., Watson, R. A., et al. 2000, ApJ, 529, 47

Halverson, N. W., Leitch, E. M., Pryke, C., et al. 2002, ApJ, 568, 38

Hanany, S., Ade, P., Balbi, A., et al. 2000, ApJ, 545, L5

Hernández-Monteagudo, C., & Rubiño-Martín, J. A. 2004, MNRAS, 347, 403

Hernández-Monteagudo, C., Genova-Santos, R., & Atrio-Barandela, F. 2004, ApJ, 613, L89

Hinshaw, G., Spergel, D. N., Verde, L., et al. 2003, ApJ, 148, 135

Hu, W., & Sugiyama, N. 1995, PhRvD, 51, 2599

Jarrett, T. H., Chester, T., Cutri, R., Schneider, S. E., & Huchra, J. P. 2003, AJ, 125, 525

Lamarre, J. M., Puget, J. L., Bouchet, F., et al. 2003, NewAR, 47, 1017L

Lee, A. T., Ade, P., Balbi, A., et al. 2001, ApJ, 561, L1

Leitch, E., Kovac, J., Halverson, N., et al. 2005, ApJ, 624, 10

Lineweaver, C. H., Barbosa, D., Blanchard, A., et al. 1997, A&A, 322, 365

Mather, J. C., Fixsen, D. J., Shafer, R. A., et al. 1999, ApJ, 512, 511

Mauskopf, P. D., Ade, P. A. R., de Bernardis, P., et al. 2000, ApJ, 536, L59

Miller, A. D., Caldwell, R., Devlin, M. J., et al. 1999, ApJ, 524, L1

Myers, A. D., Shanks, T., Outram, P. J., Frith, W. J., & Wolfendale, A. W. 2004, MNRAS, 347, L67

Netterfield, C. B., Devlin, M. J., Jarolik, N., et al. 1997, ApJ, 474, 47

Netterfield, C. B., Ade, P. A. R., Bock, J. J., et al. 2002, ApJ, 571, 604

Readhead, A., Myers, S., Pearson, T., et al. 2004, Science, 306, 836 [arXiv:astro-ph/0409569]

Rubiño-Martín, J. A., & Sunyaev, R. A. 2003, MNRAS, 344, 1155

Rubiño-Martín, J. A., Rebolo, R., Carreira, P., et al. 2003, MNRAS, 341, 1084

Sachs, R. K., & Wolfe, A. M. 1967, ApJ, 147, 73

Sievers, J. L., Bond, J. R., Cartwright, J. K., et al. 2003, ApJ, 591, 599

Smoot, G. F., Bennett, C. L., Kogut, A., et al. 1991, ApJ, 371, L1

Spergel, D. N., Verde, L., Peiris, H. V., et al. 2003, ApJ, 148, 175

Sunyaev, R. A., & Zel'dovich, I. B. 1980, ARA&A, 18, 537

Tristram, M., Patanchon, G., Macías-Peréz, J. F., et al. 2005, A&A, 436, 785

Xue, Y.-J., & Wu, X.-P. 2001, ApJ, 552, 2, 452

Yvon, D., & Mayet, F. 2005, A&A, 436, 729